Journal of Quantitative Spectroscopy & Radiative Transfer 224 (2019) 303–308

Contents lists available at ScienceDirect

Journal of Quantitative Spectroscopy & Radiative Transfer

journal homepage: www.elsevier.com/locate/jqsrt

Engineering mode hybridization in regular arrays of plasmonic nanoparticles embedded in 1D photonic crystal

V.S. Gerasimov[a,b,c,*], A.E. Ershov[a,b,c], R.G. Bikbaev[b,d], I.L. Rasskazov[e], I.V. Timofeev[f,b], S.P. Polyutov[c,b], S.V. Karpov[b,f,g]

[a] Institute of Computational Modeling SB RAS, Krasnoyarsk 660036, Russia
[b] Institute of Nanotechnology, Spectroscopy and Quantum Chemistry, Siberian Federal University, Krasnoyarsk, 660041, Russia
[c] Federal Siberian Research Clinical Centre under FMBA of Russia, Krasnoyarsk 660037, Russia
[d] Polytechnic Institute, Siberian Federal University, Krasnoyarsk 660041, Russia
[e] The Institute of Optics, University of Rochester, Rochester, NY 14627, USA
[f] Kirensky Institute of Physics, Federal Research Center KSC SB RAS, Krasnoyarsk 660036, Russia
[g] Siberian State University of Science and Technology, Krasnoyarsk 660014, Russia

ARTICLE INFO

Article history:
Received 24 August 2018
Revised 23 October 2018
Accepted 20 November 2018
Available online 22 November 2018

Keywords:
Surface lattice resonance
Photonic crystal
Optical cavity

ABSTRACT

We analytically and numerically study coupling mechanisms between 1D photonic crystal (PhC) and 2D array of plasmonic nanoparticles (NPs) embedded in its defect layer. We introduce general formalism to explain and predict the emergence of PhC-mediated Wood–Rayleigh anomalies, which spectral positions agree well with the results of exact simulations with Finite-Difference Time-Domain (FDTD) method. Electromagnetic coupling between localized surface plasmon resonance (LSPR) and PhC-mediated Wood–Rayleigh anomalies makes it possible to efficiently tailor PhC modes. The understanding of coupling mechanisms in such hybrid system paves a way for optimal design of sensors, light absorbers, modulators and other types of modern photonic devices with controllable optical properties.

1. Introduction

Hybrid systems comprised of nanoparticles (NPs) with localized surface plasmon resonance (LSPR) optically coupled to Fabry-Pérot cavities have gained a lot of attention over the last decade [1] due to their exceptional properties which can be used for narrow-band absorption [2,3], lasers [4], plasmonic loss mitigation [5], electric field enhancement [6], and sensing [7–9]. Apart from various practical implementations of Fabry-Pérot cavities, 1D photonic crystal (PhC) with defect layer represents a case of specific interest due to non-trivial coupling of NPs with PhC defect modes. The latter phenomenon may yield in improved performance of surface-enhanced Raman spectroscopy [10], ultrafast light modulation [11], PhC mode splitting [12,13], and controllable discretization of NPs optical absorption [14].

To the day, there is a number of well-established numerical procedures and theoretical models which allow to calculate electromagnetic properties of NPs embedded in half-space [15,16] or stratified media [17–20]. As a rule of thumb, resonant properties of regular 1D [21,22] or 2D [23] arrays are significantly suppressed in the presence of the substrate. Though, in the stratified medium, the existence of different coupling scenarios between plasmonic and photonic modes can be exploited in sensors [24], nanoantennas [25], and other applications [26–28].

So-called surface lattice resonances (SLRs) which have gained significant attention during the past decade [29–38] represent the case of specific interest due to their unique properties. Strong coupling between LSPRs and the grating Wood–Rayleigh anomalies [39,40] in regular arrays of NPs gives rise to remarkably narrow resonances with exceptionally high quality factor. While the most of publications study only general properties of regular NPs arrays embedded in the non-homogeneous environment, the physics behind sophisticated coupling regimes between plasmonic and photonic modes is usually hindered. The understanding of modes coupling in such systems, and the development of analytical models that predict their optical properties represent quite important applied problem.

In this paper, we study hybrid nanostructure comprised of a 1D PhC with a defect layer and a 2D periodic lattice of plasmonic Au nanodisks embedded in it. We reveal different mode hybridization scenarios by varying geometrical parameters of PhC-NPs system: radius of NPs, period of NPs array, and thickness of PhC defect

* Corresponding author at: Institute of Computational Modeling SB RAS, Krasnoyarsk 660036, Russia.
E-mail address: gerasimov@icm.krasn.ru (V.S. Gerasimov).

https://doi.org/10.1016/j.jqsrt.2018.11.028
0022-4073/

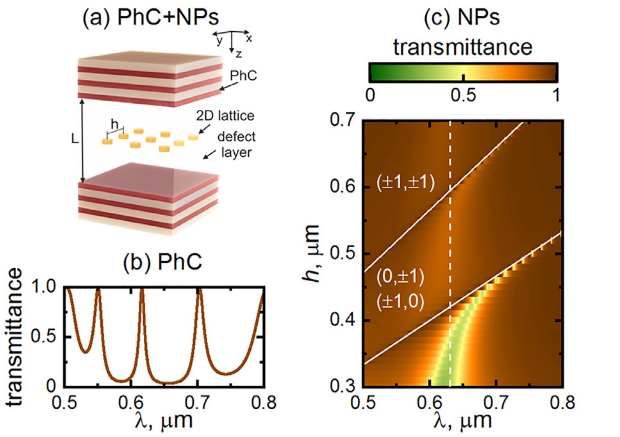

Fig. 1. (a) Schematic representation of PhC and 2D array of NPs embedded in its defect layer; (b) Transmittance of *bare* PhC with $L = 1230$ nm; (c) Transmittance of 2D lattice of Au nanodisks with height $H = 50$ nm and radius $R = 40$ nm embedded in *homogeneous* environment with $\varepsilon_{\rm def} = 2.25$. Solid lines represent Wood–Rayleigh anomalies of (p, q) order, while vertical dashed line indicates the position of dipolar LSPR of the isolated NP.

layer. We introduce theoretical model to predict the position of Wood-Rayleigh anomalies created by PhC, and to reveal possible coupling scenarios in PhC-NPs system.

2. Methods

We consider PhC with unit cell which consists of two layers: silica dioxide (SiO_2) with thickness $d_a = 120$ nm and permittivity $\varepsilon_a = 2.1$, and zirconium dioxide (ZrO_2) with thickness $d_b = 70$ nm and permittivity $\varepsilon_b = 4.16$. We assume that PhC is comprised of 6 unit cells and the defect layer (with thickness L and permittivity $\varepsilon_{\rm def} = 2.25$) in between, as shown in Fig. 1a. Regular 2D array of Au nanodisks with period h, height H and radius R is embedded in the middle of the PhC defect layer as shown in Fig. 1a. Tabulated values for ε of Au [41] have been used in simulations.

The optical properties of described structures have been calculated with commercial Finite-Difference Time-Domain (FDTD) package [42]. Nanostructures are illuminated from the top by the plane wave with normal incidence along z axis and polarization along y axis. Transmission T has been calculated at the bottom of the simulation box. Periodic boundary conditions have been applied at the lateral boundaries of the simulation box, while perfectly matched layer (PML) boundary conditions were used on the remaining top and bottom sides. An adaptive mesh has been used to reproduce accurately the nanodisk shape. Although FDTD method is a comprehensive and well-established tool which shows excellent agreement with experimental results for SLRs [33,36,43] and PhCs [44,45], extensive convergence tests for each set of parameters have been performed to avoid undesired reflections on the PMLs.

3. Results and discussion

3.1. Bare NPs array and bare PhC

Before going into details, it is instructive to briefly discuss optical response of *bare* PhC and regular array of NPs embedded in *homogeneous* medium separately. The spectral position and transmission coefficient of PhC modes can be efficiently controlled by varying layer's materials and thicknesses in PhC [46]. In this paper, PhC has the band gap from 500 to 820 nm with 3 distinct modes at 551, 617 and 703 nm, as shown in Fig. 1b. In what follows, we will refer to modes at 551 and 703 nm as odd modes, and at 617 nm as even mode. The use of this terminology is justified by odd and even number of electric field anti-nodes, respectively.

Fig. 1c explicitly shows the existence of strong coupling between LSPR and Wood–Rayleigh anomalies [39,40] in regular 2D array of NPs embedded in homogeneous environment. Such far-field coupling leads to the emergence of high-quality collective resonances [35,38] with spectral positions close to Wood-Rayleigh anomalies. In the case of normal illumination, the latter can be found with the following equation:

$$\lambda_{p,q} = h\sqrt{\frac{\varepsilon_{\rm def}}{p^2+q^2}}\ , \tag{1}$$

where p, q are integers which represent the order of the phase difference in x and y directions. Eq. (1) describes condition of constructive interference for particles within the XOY plane [47]. These anomalies of $(0, \pm1)$, $(\pm1, 0)$ and $(\pm1, \pm1)$ orders are shown in Fig. 1c. Note that λ is the *vacuum* wavelength.

3.2. Understanding mode hybridization

In the case of more complicated alignment of NPs array in PhC defect layer, additional Wood–Rayleigh anomalies emerge due to the coupling with PhC. In general case, the wavevector $\mathbf{k}$ in the defect layer reads as:

$$k^2 = k_x^2 + k_y^2 + k_z^2 = \varepsilon_{\rm def}\left(\frac{2\pi}{\lambda_{p,q,s}}\right)^2\ , \tag{2}$$

where $k_{x,\,y,\,z}$ are corresponding components of $\mathbf{k}$. The conditions of constructive interference for PhC with NPs embedded in the middle of its defect layer, can be found from:

$$k_x h = 2\pi p,\quad k_y h = 2\pi q,\quad k_z L = 2\pi s - \varphi\ . \tag{3}$$

Here s is the integer which denotes the order of the phase difference in z direction. Eq. (3) takes into account the coupling of NPs through the multiple reflections from PhC. Note that for $L \to \infty$, the coupling between NPs and PhC becomes negligible, and k_z vanishes in Eqs. (2) and (3), which yields in Eq. (1) for Wood–Rayleigh anomalies of NPs array embedded in homogeneous medium.

Eq. (3) takes into account the phase shift φ [48] that occurs due to reflection from the PhC:

$$\varphi = \arg\left[\frac{CU_{N-1}}{AU_{N-1} - U_{N-2}}\right]\ . \tag{4}$$

Here $U_N = \sin[(N+1)K\Lambda]/\sin[K\Lambda]$, $K = \arccos[(A+D)/2]/\Lambda$ is the Bloch wavenumber, $\Lambda = d_a + d_b$, and N is the number of PhC periods. A, C and D are the elements of the 2×2 $ABCD$ complex matrix which relates the amplitudes of plane waves in layer 1 of the unit cell to the corresponding amplitudes for the equivalent layer in the next PhC unit cell [48].

Although we assume that linearly polarized external radiation impinges normally on the PhC surface, the light scattered by the NPs in general case has nonzero k_x and k_y. Thus, the normal vector to the surface, the wave vector k and polarization of electric field $\mathbf{E}$ do not lie in the same plane. For this reason, in our case we have to consider both TE and TM polarizations of the electric field scattered by NPs. In this paper, we denote TE polarization as perpendicular to the plane of incidence, while TM is parallel to it.

Thus, for TE mode:

$$A = e^{ik_{az}d_a}\left[\cos k_{bz}d_b + \frac{1}{2}i\left(\frac{k_{bz}}{k_{az}} + \frac{k_{az}}{k_{bz}}\right)\sin k_{bz}d_b\right],$$

$$B = e^{-ik_{az}d_a}\left[\frac{1}{2}i\left(\frac{k_{bz}}{k_{az}} - \frac{k_{az}}{k_{bz}}\right)\sin k_{bz}d_b\right],$$

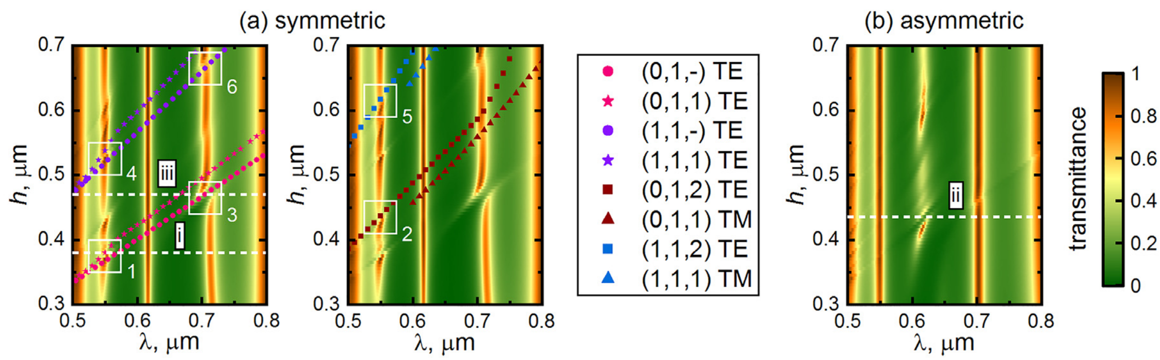

Fig. 2. Transmittance of 2D array of gold nanodisks embedded in PhC defect layer: (a) in the middle, and (b) shifted along z axis by 100 nm. Symbols denote Wood–Rayleigh anomalies of (p, q, s) order for TE and TM polarization. Note that for the convenience of the Reader, only position of strongly coupled Wood–Rayleigh anomalies are shown.

$$C = e^{ik_{az}d_a}\left[-\frac{1}{2}i\left(\frac{k_{bz}}{k_{az}} - \frac{k_{az}}{k_{bz}}\right)\sin k_{bz}d_b\right],$$
$$D = e^{-ik_{az}d_a}\left[\cos k_{bz}d_b - \frac{1}{2}i\left(\frac{k_{bz}}{k_{az}} + \frac{k_{az}}{k_{bz}}\right)\sin k_{bz}d_b\right]; \quad (5)$$

and for TM mode:

$$A = e^{ik_{az}d_a}\left[\cos k_{bz}d_b + \frac{1}{2}i\left(\frac{\varepsilon_b k_{az}}{\varepsilon_a k_{bz}} + \frac{\varepsilon_a k_{bz}}{\varepsilon_b k_{az}}\right)\sin k_{bz}d_b\right],$$
$$B = e^{-ik_{az}d_a}\left[\frac{1}{2}i\left(\frac{\varepsilon_b k_{az}}{\varepsilon_a k_{bz}} - \frac{\varepsilon_a k_{bz}}{\varepsilon_b k_{az}}\right)\sin k_{bz}d_b\right],$$
$$C = e^{ik_{az}d_a}\left[-\frac{1}{2}i\left(\frac{\varepsilon_b k_{az}}{\varepsilon_a k_{bz}} - \frac{\varepsilon_a k_{bz}}{\varepsilon_b k_{az}}\right)\sin k_{bz}d_b\right],$$
$$D = e^{-ik_{az}d_a}\left[\cos k_{bz}d_b - \frac{1}{2}i\left(\frac{\varepsilon_b k_{az}}{\varepsilon_a k_{bz}} + \frac{\varepsilon_a k_{bz}}{\varepsilon_b k_{az}}\right)\sin k_{bz}d_b\right]. \quad (6)$$

Here

$$k_{az} = \sqrt{\frac{\varepsilon_a}{\varepsilon_{\mathrm{def}}}k_z^2 + \left(\frac{\varepsilon_a}{\varepsilon_{\mathrm{def}}} - 1\right)k_x^2 + \left(\frac{\varepsilon_a}{\varepsilon_{\mathrm{def}}} - 1\right)k_y^2}\,,$$
$$k_{bz} = \sqrt{\frac{\varepsilon_b}{\varepsilon_{\mathrm{def}}}k_z^2 + \left(\frac{\varepsilon_b}{\varepsilon_{\mathrm{def}}} - 1\right)k_x^2 + \left(\frac{\varepsilon_b}{\varepsilon_{\mathrm{def}}} - 1\right)k_y^2}$$

are the wave vectors for corresponding layers of PhC.

The numerical solution of Eq. (2) for the given configuration of PhC and array of NPs (which are described in Eqs. (3) and (4)) provides the set of (p, q, s)-order Wood–Rayleigh anomalies for both TE and TM polarizations. It should be noticed, that solutions of Eq. (2) are symmetrical with respect to the following permutations and transformations: $p \leftrightarrow q$, $p \to -p$, and $q \to -q$. Thus, for convenience and without losing the generality, we consider $q \geq p \geq 0$. Due to the symmetry of the system, we limit the discussion with non-negative values of k_z and s. Finally, it should be noticed that the modes with wave vector parallel to the 2D array (i.e. with $k_z = 0$) and observed in bare NPs array are also preserved in the presence of PhC and described by Eq. (1). In what follows, we will denote such modes as $(p, q, -)$.

We would like to emphasize that the PhC-mediated interaction between Wood–Rayleigh anomalies of different orders is not taken into account in presented theoretical treatment. Such interaction can be described within the framework of vector-coupled-mode theory [49]. However, as it will be shown below, our formalism predicts positions of Wood–Rayleigh anomalies with satisfying accuracy. In the case of NPs with height H significantly smaller than the thickness of defect layer L, one could ignore the interaction between diffractive modes, though, this approximation has to be used with caution for larger NPs.

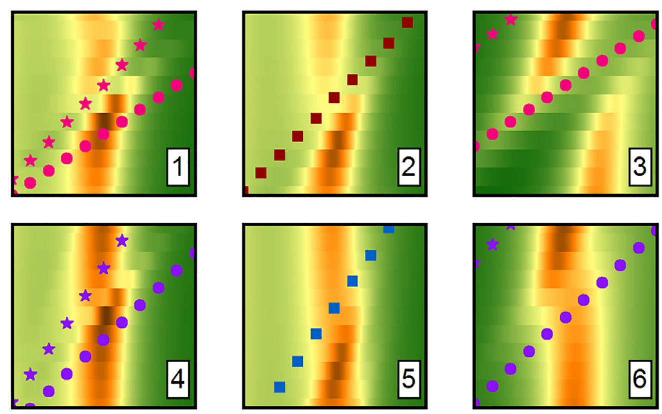

Fig. 3. Detailed illustration of various hybridization scenarios for Wood–Rayleigh anomalies shown in Fig. 2a.

3.3. Coupling scenarios between plasmonic and photonic modes

We start the discussion with NPs arrays embedded in the middle of PhC defect layer. Fig. 2a represents transmission spectra of this system for different lattice periods h. It can be seen that the multiple splittings of PhC defect modes take place for different h for odd modes only. Interestingly, even mode remains completely intact despite the fact that its frequency almost coincides with the frequency of LSPR. Fig. 3 shows detailed insets with regular Wood–Rayleigh anomalies from Fig. 1c and additional anomalies created by coupling of NPs in the array with each other via reflections from PhC. It should be mentioned that anomalies described by Eq. (1) couple with the long wavelength PhC mode only. It can be explained by strong coupling of LSPR and Wood–Rayleigh anomalies at long wavelength wing of LSPR, which is related to the behavior of dipole sum and inverse dipole polarizability of NP [31]. Figs. 2a and 3 show that PhC-mediated anomalies couple with short wavelength PhC mode only. We believe that it is also related to the behavior of the dipole sum and inverse NP polarizability.

The coupling of defect modes with Wood–Rayleigh anomalies can be controlled by moving NP array along z axis. Fig. 2b demonstrates that in the case of asymmetric alignment of NPs whose positions are shifted by 100 nm along z axis, even mode strongly couples to NP array, while odd modes exhibit weak coupling. The transmission spectra of the structure for symmetric and

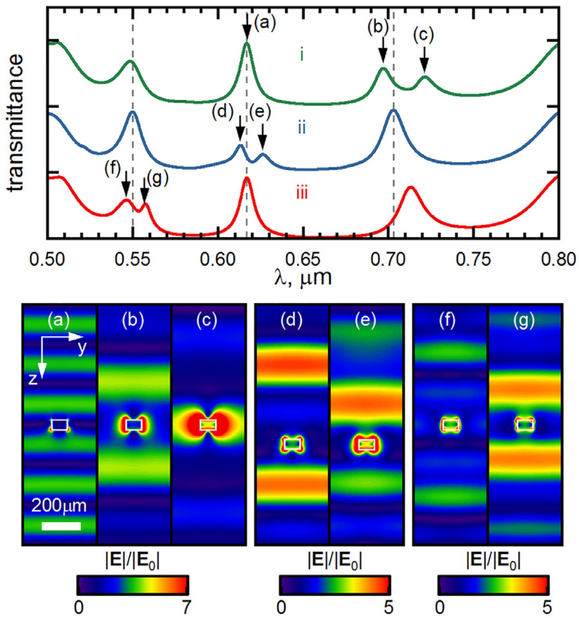

Fig. 4. (top panel) Transmission spectra for symmetric (i and iii) configuration with $h = 470$ nm and $h = 380$ nm, respectively, and for asymmetric configuration (ii) with $h = 435$ nm. Corresponding configurations are shown by white dashed lines in Fig. 2. Vertical dashed lines represent positions of PhC modes; (bottom panel) Normalized electric field distribution within the defect layer of PhC with embedded NPs for corresponding alignments (i, ii, and iii) at following wavelengths λ: (a) 617 nm; (b) 697 nm; (c) 721 nm; (d) 613 nm; (e) 626 nm; (f) 546 nm; (g) 557 nm. White rectangles denote boundaries of nanodisks. Illumination is along z axis, from the top.

asymmetric cases and different h are shown in Fig 2d. Variation of the NPs array period h allows to achieve the coupling of any PhC mode with SLR using symmetric geometry for odd PhC modes and asymmetric geometry for even modes.

The various coupling scenarios for symmetric and asymmetric alignment can be understood as follows. Let us turn to the electric field distribution within the defect layer, which is shown in Fig. 4. In the case of even mode with $\lambda = 617$ nm, the array is located in the central node of electric field (see Fig. 4a) and the coupling between the defect mode and SLR vanishes. However, for odd modes with $\lambda = 551$ and $\lambda = 703$ nm, the field is localized at the NPs (see Fig. 4b,c,f,g) and defect modes are split. The splitting of even modes can be achieved when the NPs array is located at antinode of the electric field, which is easily controlled by shifting the NPs array along z axis. The corresponding field distribution for split defect mode is shown in Fig. 4d,e.

Now let us turn to the investigation of the influence of NPs size and PhC defect layer thickness on optical properties and mode coupling scenarios in plasmonic-photonic system. The transmission spectra of the plasmonic-photonic structure for different values of R and for $h = 380$ nm are shown in Fig. 5a. In this case, splitting of the defect mode at $\lambda = 551$ nm is observed. It should be noticed that the splitting of this defect mode doesn't depend on R for $R > 40$ nm. In this case, the spectral position of the transmission maxima also does not change. This is explained by the fact that the position of the additional Wood–Rayleigh anomalies doesn't depend on the frequency of localized plasmon resonance. It should be noted that for $R > 80$ nm, a combined band gap as a superposition of the PhC band gap and the opacity region of the plasmonic array can be emerged. As a result, the width of the band gap increases roughly by half. At the same time, splitting of the defect mode is not observed when a PhC is coupled with a two-dimensional lattice of NPs with $R <$ 20nm. In this case, the wavelength of SLR doesn't coincide with the wavelength of the

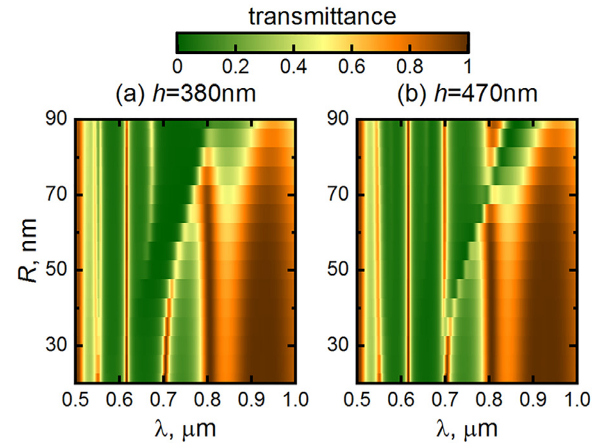

Fig. 5. Transmittance of 2D lattice of NPs with (a) $h = 380$ nm and (b) $h = 470$ nm embedded in the middle of the defect layer of PhC with $L = 1230$ nm.

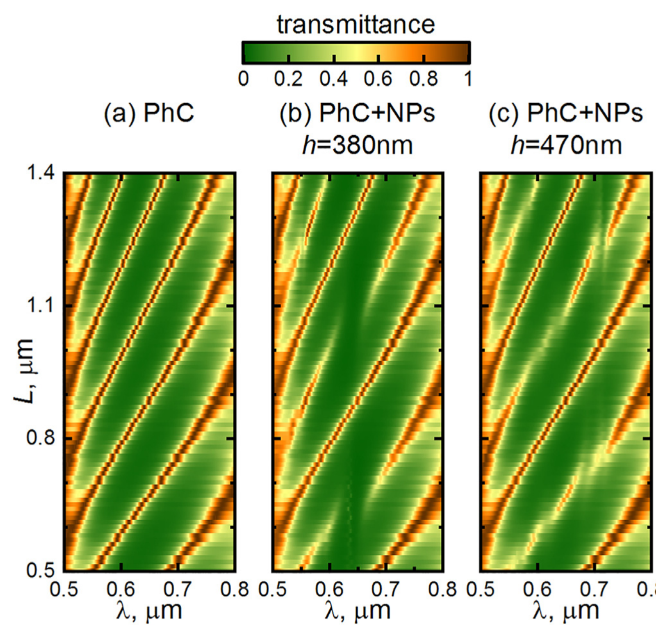

Fig. 6. Transmittance of (a) PhC without NPs; and PhC with array of NPs embedded in the middle of its defect layer for two periods h: (b) 380 nm, and (c) 470 nm.

defect mode, but falls into the frequency interval lying between the PhC defect modes with $\lambda = 617$ nm and $\lambda = 703$ nm. Finally, the even mode $\lambda = 617$ nm remains intact in all cases both for $h = 380$ nm and $h = 470$ nm, as expected from Fig. 2a, while odd mode at $\lambda = 703$ nm is significantly suppressed for $R > 50$ nm at $h = 380$ nm and around $R = 35$ nm at $h = 470$ nm (see. Fig. 5b).

The variation of the PhC defect layer thickness L is also the efficient way to control the spectral properties of PhC-NPs structure. Fig. 6 a shows that the spectral position of PhC modes slightly shifts to longer wavelength region with the increasing of L. At the same time, the number of PhC modes also increases from 2 for $L = 500$ nm to 4 for 1400 nm. Fig. 6b demonstrates that for $L = 1060$ and $L = 640$ nm, the defect modes between $\lambda = 600$ nm and $\lambda = 700$ nm can be suppressed. This suppression is explained by the fact that the wavelengths of the defect modes coincide with the wavelength of the SLR for these values of L.

Fig. 6c shows that the splitting of the PhC modes can be achieved in a wide spectral range for $h = 470$ nm. Thus, the splitting is observed at 721 nm, 632 nm, and 567 nm for $L = 1230$ nm, $L = 1050$ nm, and $L = 530$ nm, correspondingly.

4. Conclusion

To conclude, we have developed a simple yet comprehensive analytical model to explain the emergence of additional Wood–Rayleigh anomalies in 2D arrays of NPs embedded in the defect layer of 1D PhC caused by multiple reflections inside PhC. Non-trivial coupling between LSPRs in arrays of NPs and defect modes of PhC implies the existence of PhC-mediated Wood–Rayleigh anomalies which spectral positions can be defined within the framework of proposed model with reasonable accuracy. Exact simulations with the FDTD method show excellent agreement between the predicted positions of Wood–Rayleigh anomalies and regions of PhC modes hybridization. Strong coupling between PhC and NPs leads to multiple splittings of the defect modes which can be tailored by varying period h of NPs array, size of NPs, and PhC defect layer thickness. It was shown that due to the features of electric field distribution within defect layer both even and odd PhC modes can be coupled with SLR by varying the position of NPs array within it. Thus, deeper understanding of modes coupling in hybrid NPs-PhC system paves a way for more efficient control of its optical response for photonics applications which is not easy to achieve with other alternative strategies.

Acknowledgments

The reported study was funded by Russian Foundation for Basic Research, Government of Krasnoyarsk Territory, Krasnoyarsk Regional Fund of Science (Grant No.18-42-240013); by the RF Ministry of Science and Higher Education, the State contract with Siberian Federal University for scientific research in 2017–2019 (Grant No.3.8896.2017); by the Russian Science Foundation (Project No. 18-13-00363) (numerical calculations of Rayleigh anomalies in planar structures and corresponding research).

References

[1] Ameling R, Giessen H. Microcavity plasmonics: strong coupling of photonic cavities and plasmons. Laser Photon Rev 2013;7(2):141–69. doi:10.1002/lpor.201100041.
[2] Chanda D, Shigeta K, Truong T, Lui E, Mihi A, Schulmerich M, et al. Coupling of plasmonic and optical cavity modes in quasi-three-dimensional plasmonic crystals. Nat Commun 2011;2(1):477–9. doi:10.1038/ncomms1487.
[3] Liu Z, Liu G, Liu X, Huang S, Wang Y, Pan P, et al. Achieving an ultra-narrow multiband light absorption meta-surface via coupling with an optical cavity. Nanotechnology 2015;26(23):235702. doi:10.1088/0957-4484/26/23/235702.
[4] Zhou W, Dridi M, Suh JY, Kim CH, Co DT, Wasielewski MR, et al. Lasing action in strongly coupled plasmonic nanocavity arrays. Nat Nanotechnol 2013;8(7):506–11. doi:10.1038/nnano.2013.99.
[5] Kamakura R, Murai S, Ishii S, Nagao T, Fujita K, Tanaka K. Plasmonic-Photonic hybrid modes excited on a titanium nitride nanoparticle array in the visible region. ACS Photon 2017;4(4):815–22. doi:10.1021/acsphotonics.6b00763.
[6] Alrasheed S, Di Fabrizio E. Effect of surface plasmon coupling to optical cavity modes on the field enhancement and spectral response of dimer-Based sensors. Sci Rep 2017;7(1):10524. doi:10.1038/s41598-017-11140-0.
[7] Schmidt MA, Lei DY, Wondraczek L, Nazabal V, Maier SA. Hybrid nanoparticle-microcavity-based plasmonic nanosensors with improved detection resolution and extended remote-sensing ability. Nat Commun 2012;3(1):1108. doi:10.1038/ncomms2109.
[8] Bahramipanah M, Dutta-Gupta S, Abasahl B, Martin OJF. Cavity-Coupled plasmonic device with enhanced sensitivity and figure-of-Merit. ACS Nano 2015;9(7):7621–33. doi:10.1021/acsnano.5b02977.
[9] Chen J, Zhang Q, Peng C, Tang C, Shen X, Deng L, et al. Optical cavity-Enhanced localized surface plasmon resonance for high-Quality sensing. IEEE Photonics Technol Lett 2018;30(8):728–31. doi:10.1109/LPT.2018.2814216.
[10] Fränzl M, Moras S, Gordan OD, Zahn DRT. Interaction of one-Dimensional photonic crystals and metal nanoparticle arrays and its application for surface-Enhanced raman spectroscopy. J Phys Chem C 2018;122(18):10153–8. doi:10.1021/acs.jpcc.8b02241.
[11] Wang X, Morea R, Gonzalo J, Palpant B. Coupling localized plasmonic and photonic modes tailors and boosts ultrafast light modulation by gold nanoparticles. Nano Lett 2015;15(4):2633–9. doi:10.1021/acs.nanolett.5b00226.
[12] Ameling R, Dregely D, Giessen H. Strong coupling of localized and surface plasmons to microcavity modes. Opt Lett 2011;36(12):2218. doi:10.1364/OL.36.002218.
[13] Vetrov SY, Avdeeva AY, Bikbaev RG, Timofeev IV. Traveling of light through a 1D photonic crystal containing a defect layer with resonant dispersion. Opt Spectrosc 2012;113(5):517–21. doi:10.1134/S0030400X12110070.
[14] Mehrzad H, Mohajerani E. Liquid crystal mediated active nano-plasmonic based on the formation of hybrid plasmonic-photonic modes. Appl Phys Lett 2018;112(6). doi:10.1063/1.5004076.
[15] Panasyuk GY, Schotland JC, Markel VA. Short-distance expansion for the electromagnetic half-space Green's tensor: general results and an application to radiative lifetime computations. J Phys A 2009;42(27):275203. doi:10.1088/1751-8113/42/27/275203.
[16] Sikdar D, Kornyshev AA. Theory of tailorable optical response of two-dimensional arrays of plasmonic nanoparticles at dielectric interfaces. Sci Rep 2016;6(1):33712. doi:10.1038/srep33712.
[17] Paulus M, Gay-Balmaz P, Martin OJF. Accurate and efficient computation of the Green's tensor for stratified media. Phys Rev E 2000;62(4):5797–807. doi:10.1103/PhysRevE.62.5797.
[18] Egel A, Kettlitz SW, Lemmer U. Efficient evaluation of Sommerfeld integrals for the optical simulation of many scattering particles in planarly layered media. J Opt Soc Am A 2016;33(4):698. doi:10.1364/JOSAA.33.000698.
[19] Egel A, Theobald D, Donie Y, Lemmer U, Gomard G. Light scattering by oblate particles near planar interfaces: on the validity of the T-matrix approach. Opt Express 2016;24(22):25154. doi:10.1364/OE.24.025154.
[20] Egel A, Eremin Y, Wriedt T, Theobald D, Lemmer U, Gomard G. Extending the applicability of the T-matrix method to light scattering by flat particles on a substrate via truncation of sommerfeld integrals. J Quant Spectrosc Radiat Transfer 2017;202:279–85. doi:10.1016/j.jqsrt.2017.08.016.
[21] Compaijen PJ, Malyshev VA, Knoester J. Surface-mediated light transmission in metal nanoparticle chains. Phys Rev B 2013;87(20):205437. doi:10.1103/PhysRevB.87.205437.
[22] Rasskazov IL, Karpov SV, Panasyuk GY, Markel VA. Overcoming the adverse effects of substrate on the waveguiding properties of plasmonic nanoparticle chains. J Appl Phys 2016;119(4). doi:10.1063/1.4940415.
[23] Auguié B, Bendaña XM, Barnes WL, García de Abajo FJ. Diffractive arrays of gold nanoparticles near an interface: critical role of the substrate. Phys Rev B 2010;82(15):155447. doi:10.1103/PhysRevB.82.155447.
[24] Vázquez-Guardado A, Safaei A, Modak S, Franklin D, Chanda D. Hybrid coupling mechanism in a system supporting high order diffraction, plasmonic, and cavity resonances. Phys Rev Lett 2014;113(26):263902. doi:10.1103/PhysRevLett.113.263902.
[25] Lin L, Zheng Y. Optimizing plasmonic nanoantennas via coordinated multiple coupling. Sci Rep 2015;5:14788. doi:10.1038/srep14788.
[26] Nicolas R, Lévêque G, Marae-Djouda J, Montay G, Madi Y, Plain J, et al. Plasmonic mode interferences and Fano resonances in Metal-Insulator- Metal nanostructured interface. Sci Rep 2015;5(1):14419. doi:10.1038/srep14419.
[27] Shaimanov AN, Khabarov KM, Merzlikin AM, Bykov IV, Baryshev AV. Plasmon resonances in a two-dimensional lattice of metal particles in a dielectric layer: structural and polarization properties. J Exp Theor Phys 2017;124(4):584–91. doi:10.1134/S1063776117030165.
[28] Yu A, Li W, Wang Y, Li T. Surface lattice resonances based on parallel coupling in metal-insulator-metal stacks. Opt Express 2018;26(16):20695. doi:10.1364/OE.26.020695.
[29] Zou S, Schatz GC. Narrow plasmonic/photonic extinction and scattering line shapes for one and two dimensional silver nanoparticle arrays. J Chem Phys 2004;121(24):12606–12. doi:10.1063/1.1826036.
[30] Zou S, Janel N, Schatz GC. Silver nanoparticle array structures that produce remarkably narrow plasmon lineshapes. J Chem Phys 2004;120(23):10871–5. doi:10.1063/1.1760740.
[31] Markel VA. Divergence of dipole sums and the nature of non-Lorentzian exponentially narrow resonances in one-dimensional periodic arrays of nanospheres. J Phys B 2005;38(7):L115–21. doi:10.1088/0953-4075/38/7/L02.
[32] Auguié B, Barnes WL. Collective resonances in gold nanoparticle arrays. Phys Rev Lett 2008;101(14):143902. doi:10.1103/PhysRevLett.101.143902.
[33] Chu Y, Schonbrun E, Yang T, Crozier KB. Experimental observation of narrow surface plasmon resonances in gold nanoparticle arrays. Appl Phys Lett 2008;93(18):181108. doi:10.1063/1.3012365.
[34] Kravets VG, Schedin F, Grigorenko AN. Extremely narrow plasmon resonances based on diffraction coupling of localized plasmons in arrays of metallic nanoparticles. Phys Rev Lett 2008;101(8):087403. doi:10.1103/PhysRevLett.101.087403.
[35] Ross MB, Mirkin CA, Schatz GC. Optical properties of one-, two-, and three-Dimensional arrays of plasmonic nanostructures. J Phys Chem C 2016;120(2):816–30. doi:10.1021/acs.jpcc.5b10800.
[36] Khlopin D, Laux F, Wardley WP, Martin J, Wurtz GA, Plain J, et al. Lattice modes and plasmonic linewidth engineering in gold and aluminum nanoparticle arrays. J Opt Soc Am B 2017;34(3):691. doi:10.1364/JOSAB.34.000691.
[37] Zakomirnyi VI, Rasskazov IL, Gerasimov VS, Ershov AE, Polyutov SP, Karpov SV. Refractory titanium nitride two-dimensional structures with extremely narrow surface lattice resonances at telecommunication wavelengths. Appl Phys Lett 2017;111(12):123107. doi:10.1063/1.5000726.
[38] Kravets VG, Kabashin AV, Barnes WL, Grigorenko AN. Plasmonic surface lattice resonances: A Review of properties and applications. Chem Rev 2018;118(12):5912–51. doi:10.1021/acs.chemrev.8b00243.
[39] Wood RW. On a remarkable case of uneven distribution of light in a diffraction grating spectrum. Proc Phys Soc London 1902;18(1):269–75. doi:10.1088/1478-7814/18/1/325.

[40] Rayleigh L. On the dynamical theory of gratings. Proc R Soc A 1907;79(532):399–416. doi:10.1098/rspa.1907.0051.
[41] Johnson PB, Christy RW. Optical constants of the noble metals. Phys Rev B 1972;6(12):4370–9. doi:10.1103/PhysRevB.6.4370.
[42] Lumerical Solutions, “FDTD Solutions”. URL https://www.lumerical.com/tcad-products/fdtd/.
[43] Thackray BD, Thomas PA, Auton GH, Rodriguez FJ, Marshall OP, Kravets VG, et al. Super-Narrow, extremely high quality collective plasmon resonances at telecom wavelengths and their application in a hybrid graphene-Plasmonic modulator. Nano Lett 2015;15(5):3519–23. doi:10.1021/acs.nanolett.5b00930.
[44] Lavrinenko A, Borel PI, Frandsen LH, Thorhauge M, Harpøth A, Kristensen M, et al. Comprehensive FDTD modelling of photonic crystal waveguide components. Opt Express 2004;12(2):234. doi:10.1364/OPEX.12.000234.
[45] Kim JHE, Chrostowski L, Bisaillon E, Plant DV. DBR, Sub-wavelength grating, and photonic crystal slab fabry-Perot cavity design using phase analysis by FDTD. Opt Express 2007;15(16):10330. doi:10.1364/OE.15.010330.
[46] Joannopoulos JJD, Johnson S, Winn JNJ, Meade RRD. Photonic Crystals: Molding the Flow of Light. Princeton University Press; 2008. ISBN 9780691124568. doi:10.1063/1.1586781.
[47] Bonod N, Neauport J. Diffraction gratings: from principles to applications in high-intensity lasers. Adv Opt Photonics 2016;8(1):156. doi:10.1364/AOP.8.000156.
[48] Yeh P, Yariv A, Hong C-S. Electromagnetic propagation in periodic stratified media i general theory. J Opt Soc Am 1977;67(4):423. doi:10.1364/josa.67.000423.
[49] Paddon P, Young JF. Two-dimensional vector-coupled-mode theory for textured planar waveguides. Phys Rev B 2000;61(3):2090–101. doi:10.1103/PhysRevB.61.2090.